Int. J. Electrochem. Sci., 11 **(2016)** 7182 – 7197, doi: 10.20964/2016.08.61

International Journal of ELECTROCHEMICAL SCIENCE
www.electrochemsci.org

Synthesis, Characterization and Electrical Conductivity of Nano-Crystalline Erbium Sesquioxide by the Precipitation Method and Subsequent Calcination

Bahaa M. Abu-Zied[1,2,*], *Mahmoud A. Hussein*[2], *Abdullah M. Asiri*[1,2]

[1] Center of Excellence for Advanced Materials Research (CEAMR), King Abdulaziz University, P.O. Box 80203, Jeddah 21589, Saudi Arabia
[2] Chemistry Department, Faculty of Science, King Abdulaziz University, P.O. Box 80203, Jeddah 21589, Saudi Arabia
[*]E-mail: babuzaid@kau.edu.sa

Received: 28 April 2016 / *Accepted:* 15 June 2016 / *Published:* 7 July 2016

Due to its superior properties, erbium sesquioxide, Er_2O_3, is considered as an important material for applications in various fields such as corrosion-resistant coating, electrical insulating coating, in sensing membranes, semiconductor devices, as catalyst, and for applications in nuclear engineering. In the open literature there is a lack of information about the preparation of Er_2O_3 nanoparticles using the homogenous precipitation and subsequent calcination route. In this paper a facile method for the synthesis of Er_2O_3 nanoparticles is suggested. The fabrication was carried out by using the homogeneous precipitation of an erbium ions using sodium hydroxide followed by the calcination process. The influence of: (i) the pH value (9-12) during precipitation process, and (ii) the calcination temperature 300-700 °C on the structural and textural properties of the solids obtained will be addressed. The thermal events accompanying the heat treatment of the dried parent was monitored using thermogravimetric analysis (TGA). Various physicochemical techniques were used for investigating the structure and morphology of Er_2O_3 nanoparticles. These include X-ray diffraction (XRD), Fourier transform infrared (FTIR) spectra, filed emission scanning electron microscopy (FE-SEM), transmission electron microscopy (TEM), and X-ray photoelectron spectroscopy (XPS). Moreover, the electrical conductivity of the calcined samples with temperature was measured.

Keywords: nanocrystalline erbium oxide; Er_2O_3; erbium sesquioxide, electrical conductivity, precipitation method; Er_2O_3 nanoparticles

1. INTRODUCTION

Due to their unique properties such as high dielectric constant, excellent chemical, thermal and optical properties, rare earth sesquioxides are considered as promising candidates for versatility and

multi-functionality applications. These include low temperature sintering, grain growth inhibitors, superconductive applications, as phase stabilizers, solid oxide fuel cells, activators for preparation of electron trapping luminescence materials, and for applications in nuclear engineering [1-3]. As catalysts, Dy_2O_3, Ho_2O_3, Er_2O_3, Tm_2O_3, Yb_2O_3, Lu_2O_3, and Y_2O_3 showed promising activity and selectivity during vapor-phase catalytic dehydration of 1,4-butanediol to to 3-buten-1-ol [4,5] and 1,3-butanediol to 3-buten-2-ol and 2-buten-1-ol [6].

Among the various rare earth sesquioxides, Er_2O_3 is interesting because of its superior features such as high dielectric constant (≈14), high mechanical strength, high chemical and thermal stability in contact with Si, wide band gap (~5.4 eV), substantial hardness and highly transparency in visible light [7–10]. Therefore, Er_2O_3 is valuable material for applications in various fields. For instance, as protective material and in corrosion-resistant coating [11,12], as electrical insulating coating material [13], in sensing membranes for pH detection [14], and as alternative gate oxides to replace silicon oxide in complementary metal oxide semiconductor devices [15,16]. It was shown that Er_2O_3 exhibits a good catalytic performance during the oxidative dehydrogenation of ethane to ethylene [17]. Recently, it was shown that Er_2O_3 exhibits an excellent anti-permeability to hydrogen isotope to steel or other metallic structures, which may cause the destruction of these materials. In this context, Chikada et al. [18] investigated the deuterium permeation throughout Er_2O_3-Fe coatings. Their results indicated that the incorporation of Er_2O_3 increased permeation reduction by a factor over 1000 due to the crystallization of its inner layer and the oxidation of Fe-outer layer. Yang et al. [19] successfully prepared homogeneous Er_2O_3 coatings on a CLAM steel substrate by sol–gel method. Permeation experiments revealed that the Er_2O_3 coatings is a promising candidate for anti-tritium permeation in fusion reactor [19].

Erbium oxides comprise stoichiometric, ErO and Er_2O_3, and non-stoichiometric, $ErO_{1.25}$, oxides [20]. ErO can be transformed into Er_2O_3 as a result of annealing in poor vacuum [20]. $ErO_{1.25}$ is obtained by the exposure of erbium films to air [20]. Bare Er_2O_3 exists in different polymorphic structures. The cubic, C-phase, which is stable below 2600 K and is usually formed during preparation of Er_2O_3 [8]. The hexagonal Er_2O_3, H-phase, is obtained by the calcination of at temperatures higher than 2600 K [8]. The monoclinic phase, B-phase, was obtained for the first time by the pressure-induced C-phase transformation at high-temperature [20,21]. With respect to its magnetic properties, below 3.4 K Er_2O_3 is an antiferromagnetic with non-collinear structure [22]. Blanusa et al. [23] reported antiferromagnetic ↔ paramagnetic transition of Er_2O_3 at 1.8 K or lower.

Nanocrystalline materials possess an interesting physical and chemical properties, which are different from their bulk counterparts, such as low density, smaller particles size, large surface area, stability, etc. Several methods have been reported for the preparation of nano-crystalline Er_2O_3. In this way, sphere-like Er_2O_3 nanoparticles were prepared by the sol-gel method [17,24] as well as the glycothermal treatment of erbium acetate and subsequent calcination [25]. Irregular shape ultrafine-Er_2O_3 nanoparticles were prepared by the thermal decomposition of erbium 2,4-pentadione complex [23]. Radio frequency magnetron sputtering technique was used to prepare Er_2O_3 thin films with thickness of 200-1000 nm [26]. Homogenous precipitation and subsequent calcination method is a simple, template-free, flexible and promising technique for the preparation of nanomaterials. This method has been successfully used for the preparation of nano-crystalline Pr_6O_{11} [27], Dy_2O_3 [28], and

Tb_4O_7 [29]. Accordingly, the idea of the present investigation seeks to prepare erbium oxide, Er_2O_3, nanoparticles using the precipitation method employing NaOH as precipitant and subsequent calcination at 500 °C. Preliminary experiments focused on the influence of the pH value (9, 10.5 and 12) on the morphology and crystallite size of the will obtained Er_2O_3 nanoparticles. For the Er_2O_3 with lowest crystallite size, which was prepared using pH = 12.0, the study has been extended to investigate the effect of calcination temperature on its structural as well as textural features at the temperature range of 300-700 °C. Various characterization techniques have been employed including TGA, XRD, FTIR, FE-SEM, TEM and XPS. Moreover, the electrical conductivity of the samples calcined at different temperatures was measured.

2. EXPERIMENTAL

2.1. Preparation of Er_2O_3 nanoparticles

Analytical grade chemicals, commercial Er_2O_3, HNO_3, and NaOH, were the reagents employed in the present investigation and they were used without further purification. Two series of Er_2O_3 samples were prepared using the precipitation method. In the first one, we have investigated the influence of the pH value on the particle size of the obtained nano-crystalline Er_2O_3. Briefly, 2 g of commercial Er_2O_3 was dissolved in dilute HNO_3 with heating, which resulted in the formation of a pale pink solution of $Er(NO_3)_3$. Then, NaOH (2 *M*) solution of was added dropwise to the $Er(NO_3)_3$ solution with vigorous stirring until a pH value of 9.0 was reached. The pink precipitate obtained was stirred for 30 min, then filtered using centrifuge, and washed with distilled water several times until the pH value of the filtrate reached about. The pink solid obtained was dried at 40 °C for three days. Finally, the dried product was calcined at 500 °C for 1 h. Two other samples were prepared using the same procedure by keeping the pH during the precipitation process at 10.5 and 12. In the second series, we have investigated the influence of the calcination temperature change, 300 -700 °C, on the phase formation and the crystallite size of Er_2O_3 nanoparticles. The working procedure employed in the preparation of this series was similar to that used of the former one, where a pH value was adjusted to 12.0 during the precipitation. The selection of pH value of 12.0 during the precipitation of the samples of this series was attributed to the fact that this pH has led to the formation of Er_2O_3 with the smallest crystallites size (vide infra).

2.2. Instrumentation

Thermogravimetric analysis of the dried parent (DTA/DTG) was conducted on a TA instrument apparatus (model TGA-Q500) from ambient till 950 °C using a heating rate of 5 °C min^{-1} in nitrogen flow (40 ml min^{-1}). FT-IR (4000–400 cm^{-1}) was recorded on the Nicolet iS50 FT-IR spectrometer using Attenuated Total Reflectance (ATR) sampling accessory. Phase analysis of the Er_2O_3 nanoparticles was performed by powder XRD using Thermo-Scientific ARL X'TRA Powder Diffractometer with Cu Kα radiation ($\lambda = 1.5418$ Å). The surface morphology and the microstructure were examined by (i) a field emission scanning electron microscope (JEOL model JSM-7600F)

equipped with EDS (energy dispersive spectroscopy) system, and (ii) transmission electron microscopy (TEM, model JEM1011). The X-ray photoelectron spectroscopy (XPS) analysis was performed on a Thermo Scientific K-Alpha KA1066 X-ray photoelectron spectrometer, using a standard dual-anode excitation source emitting monochromatic Al-Kα (1486.6 eV) radiation. The electrical conductivity of the calcined Er_2O_3 nanoparticles was measured using Keithley 6517A electrometer. In each run a 0.5 g of the sample powder was pressed between two silver electrodes (1.0 cm diameter), then placed in the conductivity Pyrex glass cell placed in a tube furnace, where its temperature was controlled using a digital temperature controller. The conductivity values were measured with the temperature.

3. RESULTS AND DISCUSSION

3.1. Characterization of the dried Er-parent

Fig. 1(a) shows the XRD pattern of the solid product dried obtained by the precipitation of Er^{3+} ions using NaOH at pH of 9.0. The pattern indicates the presence of one peak at $2\theta = 25.40°$ and two other broader peaks at $2\theta = 27.50\text{-}38.0°$ and 38.0-70.0°. These observations indicates the amorphous nature of the obtained material. Moreover, these reflections did not match with the standard JCPDS cards for erbium hydroxide. FT-IR spectrum of the Er-parent (Fig. 1(b)) shows the presence of absorptions at 670, 850, 1084, 1383, 1530, 1644 and 3450 cm^{-1}. The absorptions at 1530, 1383, 1084, 850 and 670 cm^{-1} can be assigned to the ν_5, ν_1, ν_2, ν_8, ν_6 normal vibrational bands for carbonate group in erbium carbonate, respectively [30–32]. The two bands located at 1644 and 3450 cm^{-1} can be assigned to the O–H bending and stretching vibration modes, respectively [33]. This picture suggests that the obtained parent is hydrated carbonate or hydroxy-carbonate of erbium. In this context, different methods have been employed in the preparation of rare earth carbonates with various structures. The common method utilized is the reaction of the carbonate or bicarbonate anions with an aqueous solution of the rare earth ions [30–32,34]. Other preparation routes involve the reaction of urea with an aqueous solutions of rare earth ions at ~ 90 °C [32] or the hydrolysis of these rare earth trichloroacetates [34]. Yanagihara et al. [31] successfully prepared La^{3+}, Nd^{3+}, Sm^{3+}, Eu^{3+}, Gd^{3+}, Dy^{3+} and Ho^{3+} normal carbonates by the reaction of the corresponding oxides suspensions of these ions with CO_2 under supercritical conditions (68–240 atm). Concurrently, Caro et al. [35] prepared holmium and erbium carbonates by the vigorous stirring of a water suspension of their oxide powders under a CO_2 atmosphere. Michiba et al. [36] prepared a series of $RE(CO_3)OH$, RE = La, Pr, Nd, Sm, Eu, Gd, Tb, Dy, Ho, and Er, hydrothermally in alkaline medium.

FE-SEM inspection of the dried Er-parent reveals the presence of a porous network covering the surface of this solid, which exhibit cauliflower-like structure (Fig. 1 (c)). The relevant EDX pattern of the Er-parent (Fig. 1 (d)) indicates that it is composed of Er, C, and O atoms with mass% ratios of 57.15:13.20:29.65, respectively. Accordingly, we may explain the formation of erbium carbonate as expressed by the following equations:

$$NaOH \rightarrow Na^+ + OH^- \quad \text{..... (1)}$$

$$CO_2 + H_2O \leftrightarrow H_2CO_3 \quad \text{..... (2)}$$
$$H_2CO_3 \leftrightarrow H^+ + HCO_3^- \quad \text{..... (3)}$$
$$HCO_3^- \leftrightarrow H^+ + CO_3^{2-} \quad \text{..... (4)}$$
$$Er^{3+} + OH^- + CO_3^{2-} + xH_2O \rightarrow ErOHCO_3 \cdot xH_2O \quad \text{..... (5)}$$

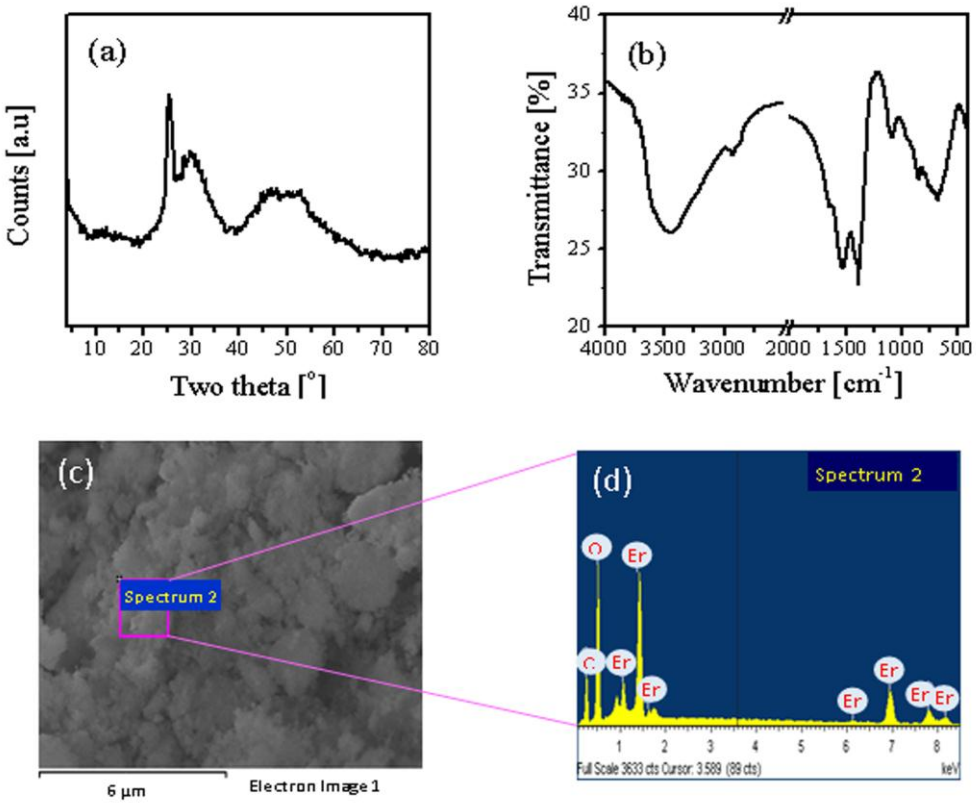

Figure 1. XRD (a), FT-IR (b), FE-SEM (c) and EDX (d) of the dried Er-parent prepared by the precipitation rout at pH of 9.0.

TGA thermograph of the dried Er-parent is shown in Fig. 2. The first weight loss step in this thermograph extends from ambient till around 195 °C and maximized at 93 °C. The obtained weight loss in this step is amount to 12.05 %. This step plausibly could be related to the dehydration of erbium hydroxy-carbonate. Accordingly, the formula $ErOHCO_3 \cdot 1.25H_2O$ can be proposed and the dehydration of this parent could proceed as follows:

$$2ErOHCO_3 \cdot 1.25H_2O \rightarrow 2ErOHCO_3 + 2.5\ H_2O \quad \text{..... (6)}$$
$$2ErOHCO_3 \rightarrow Er_2O(CO_3)_2 + H_2O \quad \text{..... (7)}$$

Fig. 2 shows the presence of a consecutive steps, which are maximized at 232 °C and 534 °C. These steps are accompanied by a total weight loss of 15.78 %, which is close to that 16.5 % anticipated to the removal of CO_2 molecules according to:

$$Er_2O(CO_3)_2 \rightarrow Er_2O_2CO_3 + CO_2 \quad \text{..... (8)}$$
$$Er_2O_2CO_3 \rightarrow Er_2O_3 + CO_2 \quad \text{..... (9)}$$

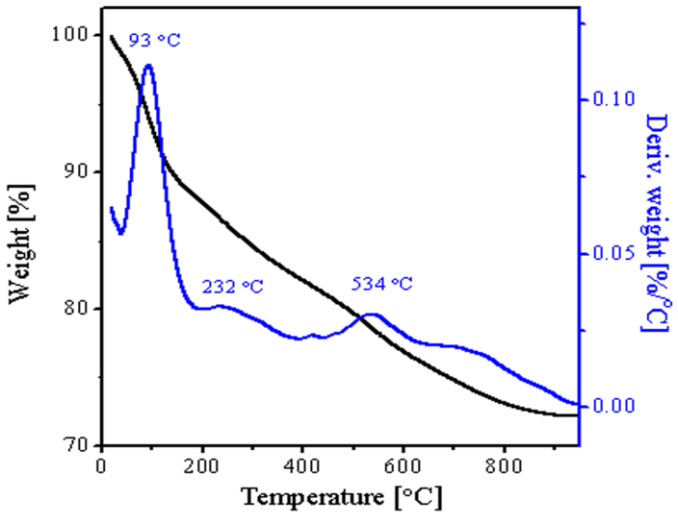

Figure 2. TGA thermograph of the dried erbium parent prepared at pH = 9.0.

3.2. Effect of pH

To gain insight to the effect of pH on the morphology and crystallite size of Er_2O_3 nanoparticles, a combined XRD, FE-SEM, TEM and XPS analyses have been performed. XRD patterns of Er_2O_3 nanoparticles prepared at different pH values and calcined at 500 °C are presented in Fig. 3. Inspection of this figure reveals that all the three samples exhibit similar XRD patterns. Moreover, all the obtained reflections in these patterns can be indexed as crystalline cubic Er_2O_3 (JCPDF file 77-0777). The magnified part of the strongest reflection (2θ at 29.11 – 29.29) in Fig. 3 reveals a shift of that reflections towards left with the pH value of the preparation increase i.e. 2θ decreases. Table 1 lists the diffraction data for the Er_2O_3 samples prepared at pH values of 9.0, 10.5 and 12.0 and calcined at 500 °C. From the inspection of these data it appears that all the diffraction peaks exhibit 2θ shift with the pH value increase. The extent of this 2θ shift increases with the pH as well as 2θ increase. The Bragg Equation (2 d sin θ = n λ) indicates that decreasing θ value results in the increase of the inter-planar distance (d). Table 1 indicates that the observed shift in the 2θ values towards lower values is accompanied by an increase in the corresponding inter-planar distances. In other words, increasing the pH value during the samples preparation is accompanied by a lattice expansion of the prepared Er_2O_3 nanoparticles. This finding indicates the sensitivity of Er_2O_3 to the pre-synthesis treatments. In the literature there are several papers reporting the lattice expansion of Er_2O_3 as a result of the pre- and post-synthesis treatments. For instance, an inter-planar distance increase was reported upon increasing the Er_2O_3 mole % in the ZrO_2-Er_2O_3 [37] and ThO_2-Er_2O_3 [38] systems. More recently, a lattice expansion of Er_2O_3 was obtained after high-temperature deuterium permeation experiments [39]. The crystallite size of the three Er_2O_3 samples was estimated using Sherrer equation, d = 0.9 λ / β cos θ, where λ is the X-ray excitation wavelength, β is the experimental full width at half maximum for the strongest reflection (2θ at 29.11 – 29.29) and θ is the Bragg angle. The calculated sizes were 21, 23 and 19 nm for the samples prepared at pH values of 9.0, 10.5 and 12.0, respectively.

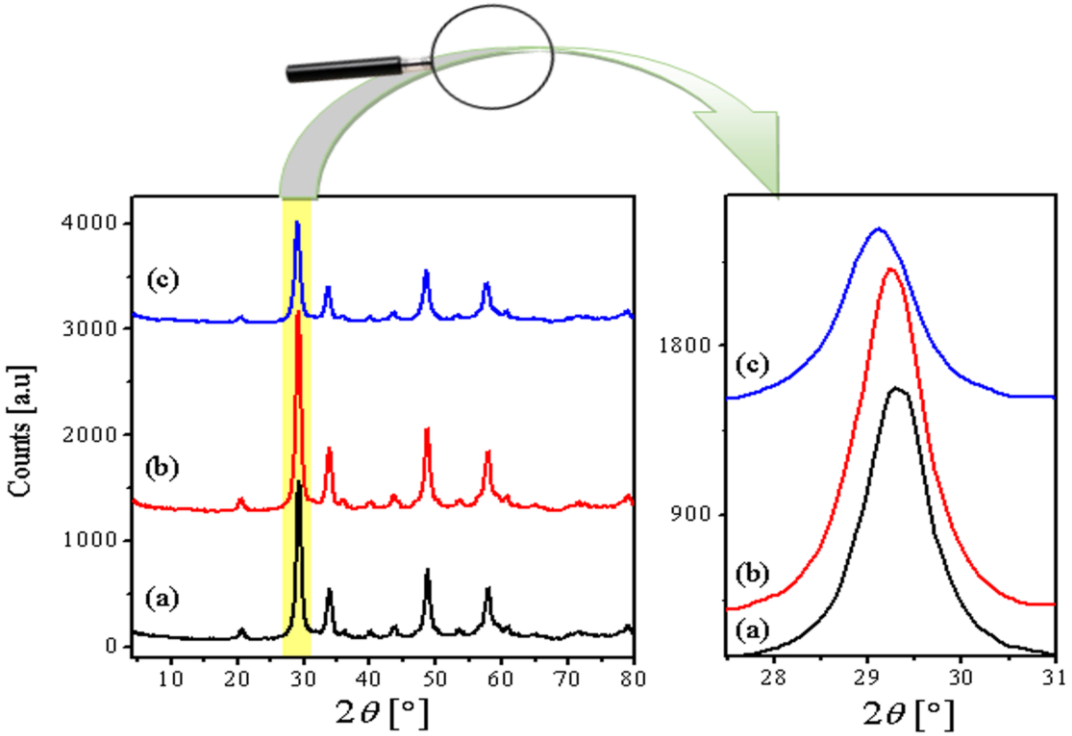

Figure 3. X-ray powder diffraction patterns of Er_2O_3 prepared at pH = 9 (a), 10.5 (b) and 12 (c) and calcined at 500 °C.

Table 1. JCPDS and experimental data h k l, diffraction peak positions, inter-planer distance (d) values of the cubic Er_2O_3 prepared by the precipitation method at pH values of 9.0, 10.5, and 12.0 and calcined at 500 °C.

(h k l)	$2\theta_{liter.}$ [°]	$d_{liter.}$ [nm]	Sample preparation pH value					
			9.0		10.5		12.0	
			$2\theta_{exp.}$ [°]	$d_{exp.}$ [nm]	$2\theta_{exp.}$ [°]	$d_{exp.}$ [nm]	$2\theta_{exp.}$ [°]	$d_{exp.}$ [nm]
2 1 1	20.63	4.301	20.60	4.308	20.54	4.320	20.42	4.345
2 2 2	29.34	3.041	29.29	3.046	29.23	3.052	29.11	3.065
4 0 0	34.00	2.634	33.91	2.641	33.85	2.645	33.73	2.655
4 4 0	48.87	1.863	48.77	1.865	48.71	1.867	48.53	1.874
6 2 2	58.03	1.588	57.94	1.590	57.88	1.591	57.64	1.597

liter. = literature, exp. Experimental, d = inter-planar distance

Fig. 4 depicts the surface morphology of Er_2O_3 samples prepared at pH = 9.0-12 and calcined at 500 °C as investigated by FE-SEM. All the three samples show a porous morphology resulting from the gases (H_2O and CO_2) emerging during the calcination process. Similar morphology is exhibited by the two samples prepared using pH = 9.0 and 10.5, which are characterized by the presence of irregular shaped particles, which contain foam-like structures distributed among them. The sample prepared at pH = 12.0, on the other hand, consists of agglomerations of nearly sphere-shaped particles, which contain narrower pores.

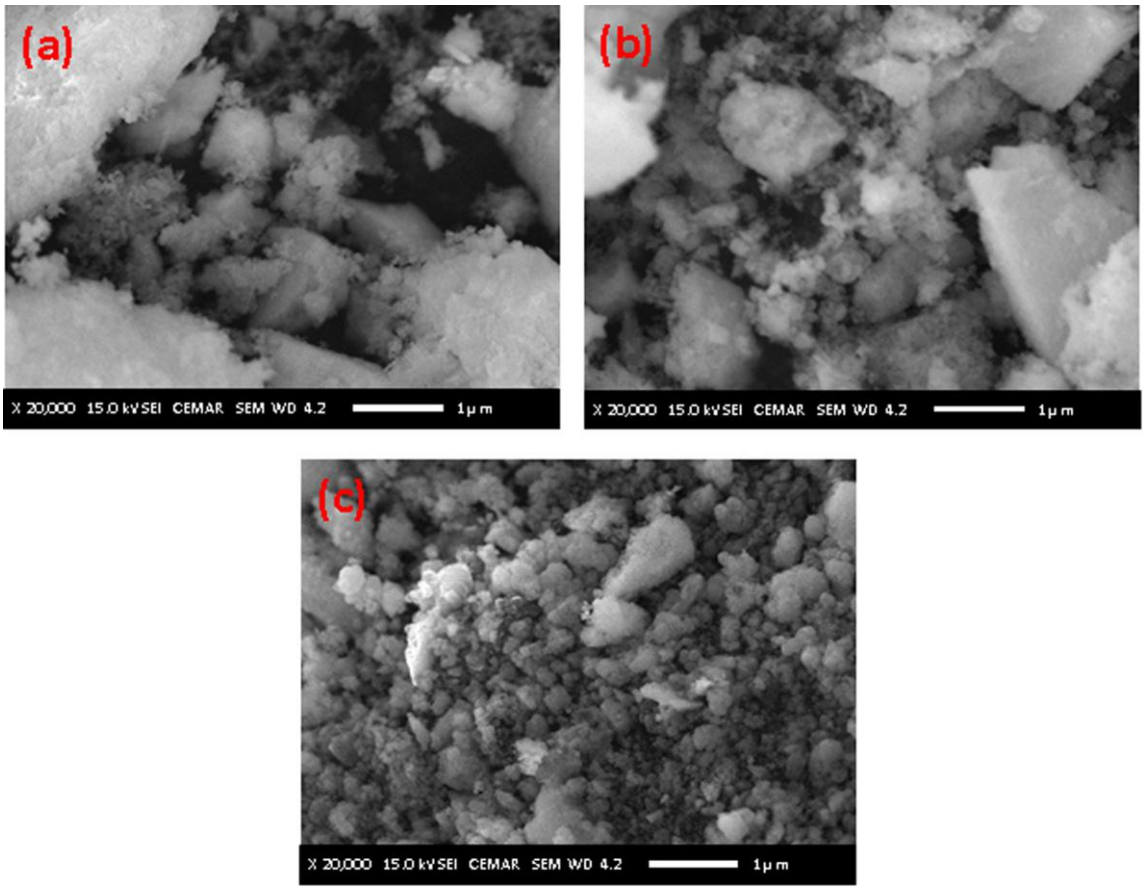

Figure 4. FE-SEM photographs of Er_2O_3 prepared at pH = 9 (a), 10.5 (b) and 12 (c) and calcined at 500 °C.

The relevant TEM nanographs of these Er_2O_3 samples are presented in Fig. 5. The image of the sample prepared at pH = 9.0 (Fig. 5 (a)) shows a nano rod-like crystals with uniform diameters (9-13 nm) and lengths in the range 35-100 nm. Increasing the pH value to 10.5 during the preparation procedure clearly results in the production of nano rod-like Er_2O_3 crystals with larger dimensions as shown in Fig. 5(b). A dramatic morphological change was obtained upon increasing the precipitation pH value to 12 (Fig. 5(c)). Obviously, such treatment induces a rod-like → sphere-like transformation. The obtained particle have diameters in the range 7-13 nm. This morphology difference between the samples prepared at different pH value clearly indicates the high sensitivity of Er_2O_3 nanoparticle to the pre-synthesis conditions.

The XPS spectra were performed to examine the chemical surface composition and oxidation state of the prepared Er-samples. The obtained Er $4d_{5/2}$ and O 1s XPS spectra of the Er_2O_3 samples being prepared at different pH values are presented in Figs. 6(A) and 6(B), respectively. Fig. 6(A) reveals two characteristic spectral features Er $4d_{5/2}$. The firs one appears at binding energy close to 169 eV, which is close to that (168.3-169 eV) reported for Er_2O_3 sesquioxide [14,40–44]. The second feature appears at 175.00 eV, which is shifted to 179.46 eV on increasing the pH to 12.0. Due to the insufficient information about the XPS spectra of erbium carbonate in the literature and from the fact that various RE oxides tend to form surface carbonates, by reaction with CO_2, on the exposure to atmospheric air [45,46]; we may relate this feature to Er^{3+} in erbium surface carbonate. The O 1s

spectrum of the Er_2O_3 sample prepared at pH = 10.5 (curve b in Fig. 6(B)) shows two peaks at 532.48 and 538.22 eV. This first one could be attributed to Er–O groups [41,44], whereas the second component is close to that ascribed to C–O species [46]. Increasing the pH value during the Er_2O_3 preparation shifts these two peaks to 533.51 and 541.14 eV, respectively. On the other hand, decreasing the preparation pH value to 9.0 leads to a merge of these two component in one broad peak at BE value of 535.56 eV.

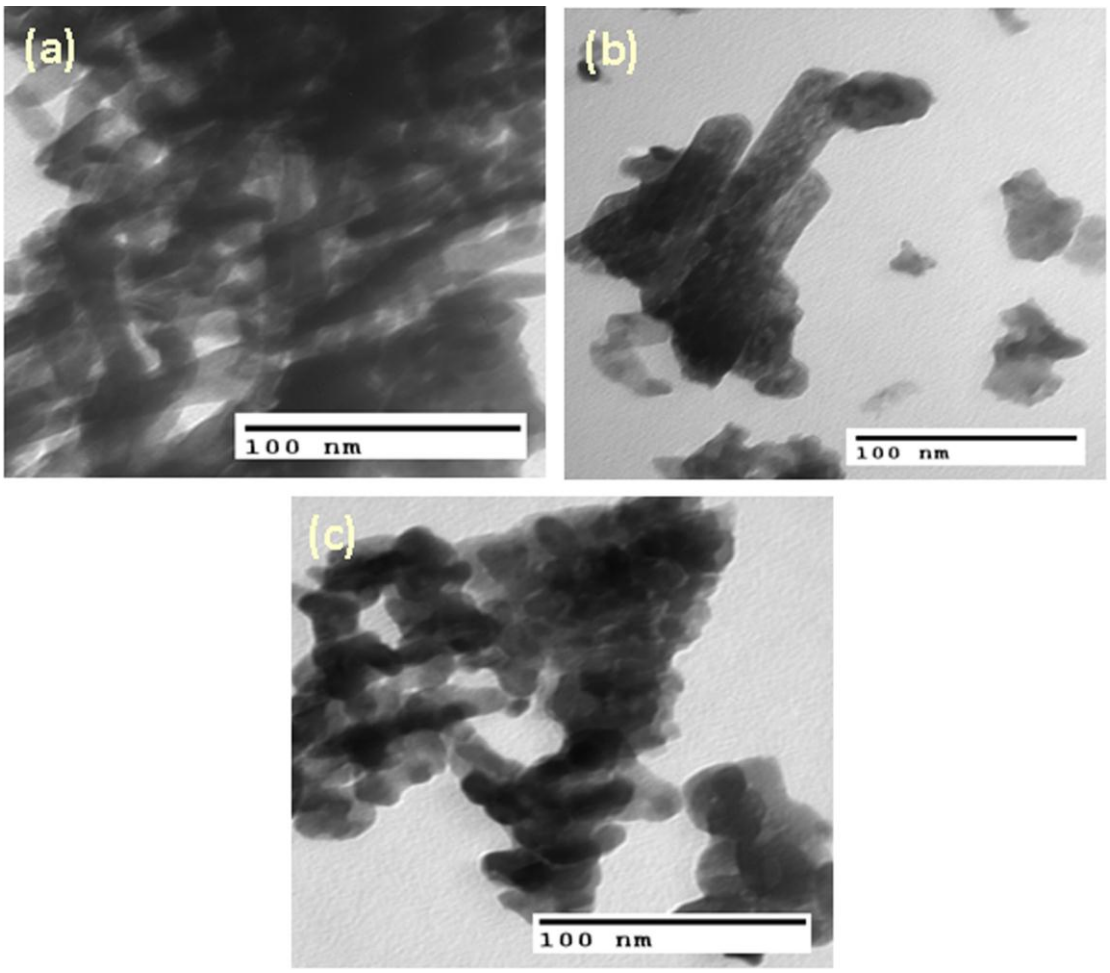

Figure 5. TEM pictures of Er_2O_3 prepared at pH = 9 (a), 10.5 (b) and 12 (c) and calcined at 500 °C.

3.3. Effect of calcination temperature

In this section we will present the results of changing the calcination temperature on the physico-chemical properties of Er_2O_3 prepared using pH = 12.0, which possesses the smallest crystallites size. The XRD patterns of the erbium precursor calcined at the temperature range of 300–700 °C are shown in Fig. 7. Heating the Er-precursor at 300 °C leads to the formation of an amorphous solid material. Calcining the Er-precursor at 400 °C is accompanied by an emergence of new reflections match well with those of the cubic Er_2O_3 (JCPDF file 77-0777) with lattice constant "*a"* of 10.5360 nm. Further raise in the calcination temperature till 700 °C leads to an increase in the intensity of all reflection due to Er_2O_3 phase.

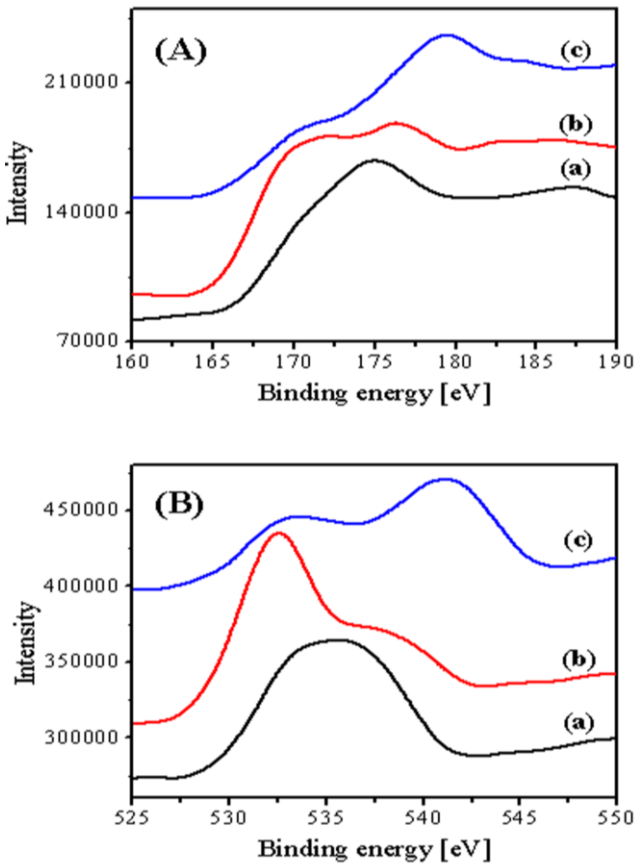

Figure 6. Er $4d_{5/2}$ (A) and O 1s (B) XPS spectra of the Er_2O_3 samples being prepared at pH = 9.0 (a), 10.5 (b), and 12.0 (c).

The magnified section of the strongest Er_2O_3 reflection (Fig. 7) shows a gradual shift towards higher 2θ values with the calcination temperature raise. The diffraction data for the calcined Er_2O_3 samples are listed in Table 2. It is obvious that all the diffraction peaks are shifted towards higher values as a result of raising the calcination temperature. Table 2 shows that the calculated inter-planar distance (d) decreases as the calcination temperature and the 2θ increased. The Sherrer-estimated crystallite size values were 17.5. 19.0, 19.8 and 23.0 nm for the Er_2O_3 samples calcined at 400, 500, 600 and 700 °C, respectively.

Table 2. JCPDS and experimental data h k l, diffraction peak positions, inter-planer distance (d) values of the cubic Er_2O_3 prepared by the precipitation method at pH value of 12.0 and calcined at 400, 500, 600 and 700 °C.

(h k l)	$2\theta_{lit.}$ [°]	$d_{lit.}$ [nm]	Sample calcination temperature [°C]							
			400		500		600		700	
			$2\theta_{exp.}$ [°]	$d_{exp.}$ [nm]	$2\theta_{exp.}$ [°]	$d_{exp.}$ [nm]	$2\theta_{exp.}$ [°]	$d_{exp.}$ [nm]	$2\theta_{exp.}$ [°]	$d_{exp.}$ [nm]
2 1 1	20.63	4.301	20.36	4.358	20.42	4.345	20.54	4.320	20.60	4.308
2 2 2	29.34	3.041	28.99	3.077	29.11	3.065	29.29	3.046	29.31	3.044
4 0 0	34.00	2.634	33.67	2.659	33.73	2.655	33.91	2.641	33.98	2.636
4 4 0	48.87	1.863	48.47	1.876	48.53	1.874	48.77	1.865	48.83	1.863
6 2 2	58.03	1.588	57.58	1.599	57.64	1.597	57.88	1.591	57.94	1.590

lit. = literature, exp. Experimental, d = inter-planar distance

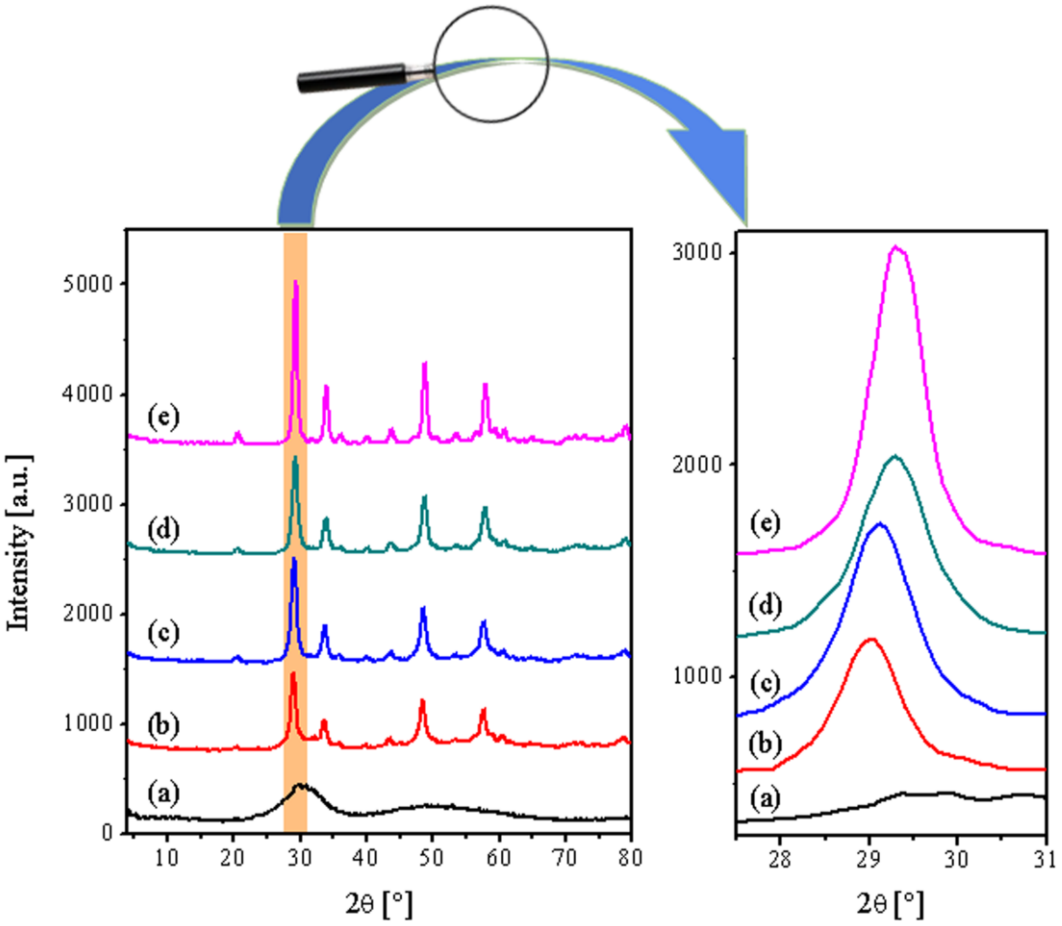

Figure 7. X-ray powder diffraction patterns of Er_2O_3 prepared at pH = 12 calcined at 300 °C (a), 400 °C (b), 500 °C (c), 600 °C (d) and 700 °C (e).

Fig. 8 depicts the FE-SEM photographs of erbium samples calcined at 400 and 700 °C. Fig. 8(a) reveals that the 400 °C calcined sample possesses a porous morphology resulting from the gases evolved during the calcination process. Moreover, the particles of this sample show an irregularly shaped agglomerates.

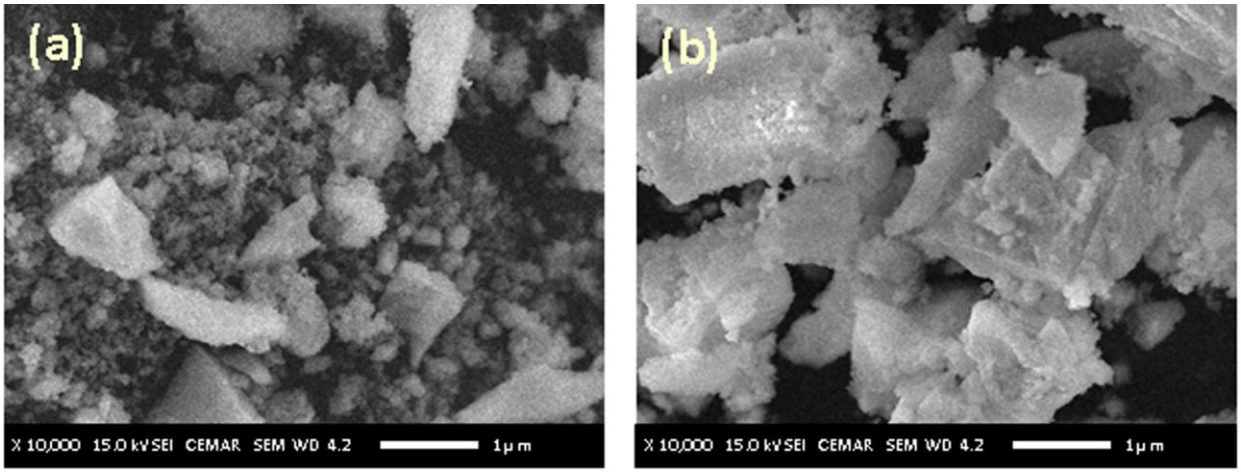

Figure 8. FE-SEM photographs of Er_2O_3 prepared at pH = 12 and calcined at 400 °C (a) and 700 °C (b).

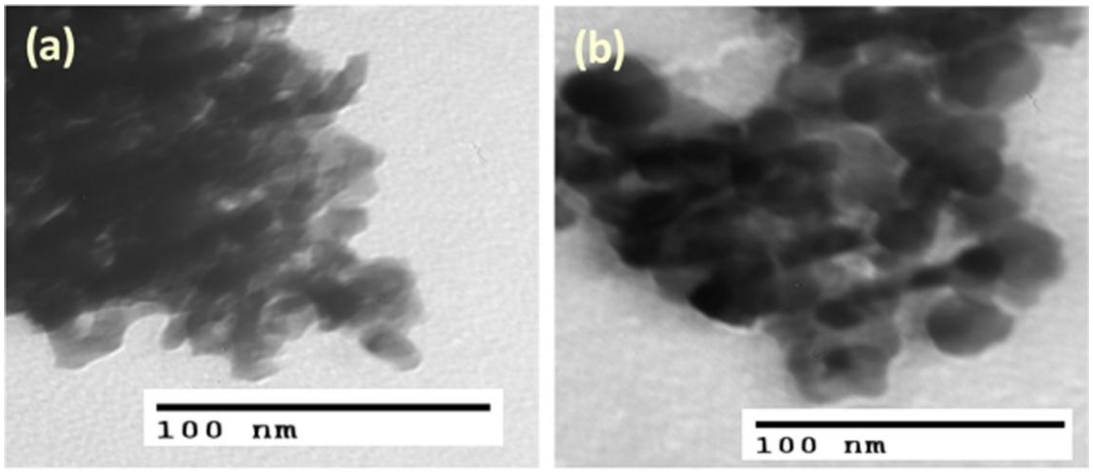

Figure 9. TEM photographs of Er_2O_3 prepared at pH = 12 and calcined at 400 °C (a) and 700 °C (b).

Raising the calcination temperature to 700 °C (Fig. 8(b)) is associated with an elimination of the inter-particles voids and the formation of aggregates with flake-like morphology. TEM nan-graph of the 400 °C calcined sample (Fig. 9(a)) reveals that it is composed of welded sphere-like particles with diameters in the range 16–19 nm. Similar morphology is exhibited by the 700 °C calcined sample (Fig. 9(b)), where larger particles (18–31 nm) can be observed.

Fig. 10 shows the XPS spectra of the Er_2O_3 samples obtained by calcining the Er-precursor at 400 and 700 °C for 1 h. Inspection of the Er $4d_{5/2}$ spectra shown in Fig. 10(A) reveals the following two points: (i) erbium sesquioxide as well as erbium carbonate coexist on the surface of the 400 °C calcined sample as judged from the appearance of the two peaks at 169.66 and 178.63 eV, respectively, and (ii) the 700 °C calcined sample showed the persistence of the peak due to erbium sesquioxide and the disappearance of the peak due to erbium carbonate. In this context, our XRD data (Fig. 7) indicated that Er_2O_3 is the only phase detected for the samples calcined at the 400–700 °C range. The detection of erbium carbonate for the 400–500 °C calcined sample is not surprising, since XPS is a surface technique whereas XRD is a bulk analysis tool. The XPS spectra of the O 1s level for the 400 and 700 °C calcined samples are shown in Fig. 10(B). Spectrum (a) in this figure shows two peaks at BE values of 532.38 and 541.00 eV. Following the previous assignments for the XPS data presented in Fig. 6(B), these two peaks could be related to Er–O [41,44] and C–O [46] species, respectively. Calcining the Er-precursor at 700 °C has led to the disappearance of the peak at 541.00 eV, which indicates a dissimilar oxygen bonding environment to that of the 400 °C calcined material. In other words, the surface of the 700 °C sample contains Er_2O_3 phase only, where erbium carbonate is completely decomposed. This finding is a further confirmation for the 541.00 eV peak to erbium carbonate phase. Electrical conductivity measurement was performed as an additional tool to characterize the 300–700 °C calcined samples. The experiments were carried out at the 200–500 °C range. In Fig. 11, the natural logarithm of the σ as a function of the calcination temperature plots are shown at various measuring temperatures.

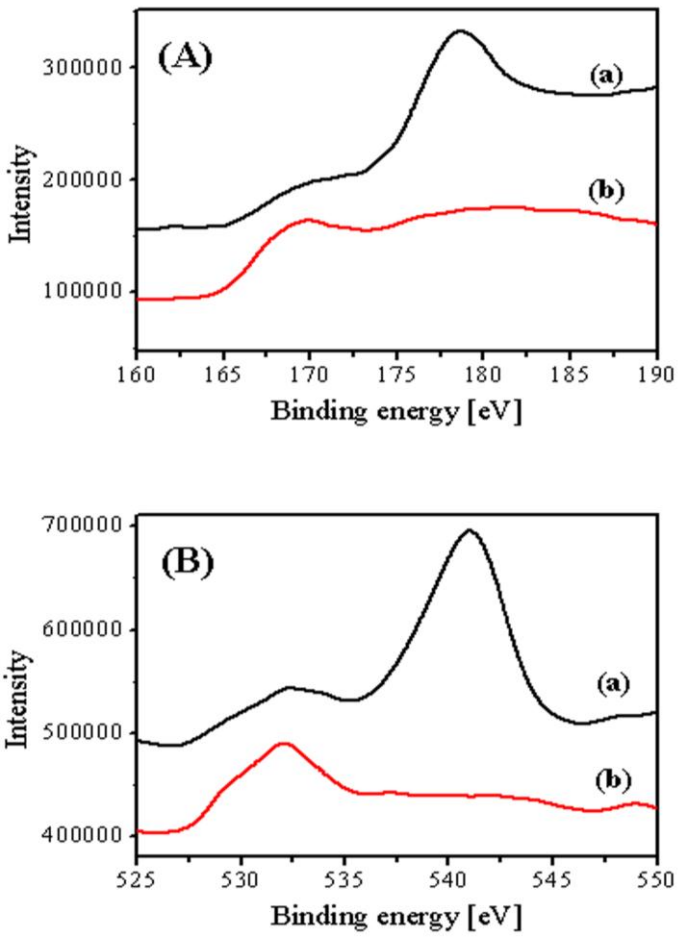

Figure 10. Er $4d_{5/2}$ (A) and O 1s (B) XPS spectra of the Er_2O_3 samples being prepared at pH = 12.0 and calcined at 400 °C (a) and 700 °C (b).

The obtained results show that the mode of conductivity variation with the pre-treatment temperature is the same for all the measured temperatures (200–500 °C). The picture shown in Fig. 11 can be understood taking into account the previously discussed characterizations results. Maximum conductivities are exhibited by the 300 °C calcined sample. A drop in the conductivity can be observed as result of calcining the Er-precursor at 400 °C. This drop corresponds to the Er_2O_3 phase formation, which was confirmed by the XRD measurements (Fig. 7). In other words, the amorphous erbium carbonate, which is the constituent of the 300 °C calcined sample, is characterized by higher conductivity of the erbium sesquioxide. It is known that the oxides that crystallize in the fluorite structure (such as stabilized ZrO_2 and ThO_2) exhibit O^{2-} ion conduction. It was reported that the rare earth oxides with type-C structure can be considered as a modified fluorite structure. Erbium sesquioxide is the common known solid oxide, which has the rare earth type-C structure up to 2280 °C [47].

Yo et al. [48] demonstrated that the electrical conductivity of erbia increase with both the temperature and the oxygen partial pressure. Won et al. [37] reported a conductivity decrease upon increasing the Er mol % in the ZrO_2-Er_2O_3 system. Fig. 11 shows that further raise in the calcination temperature till 700 °C is accompanied with a continuous conductivity decrease.

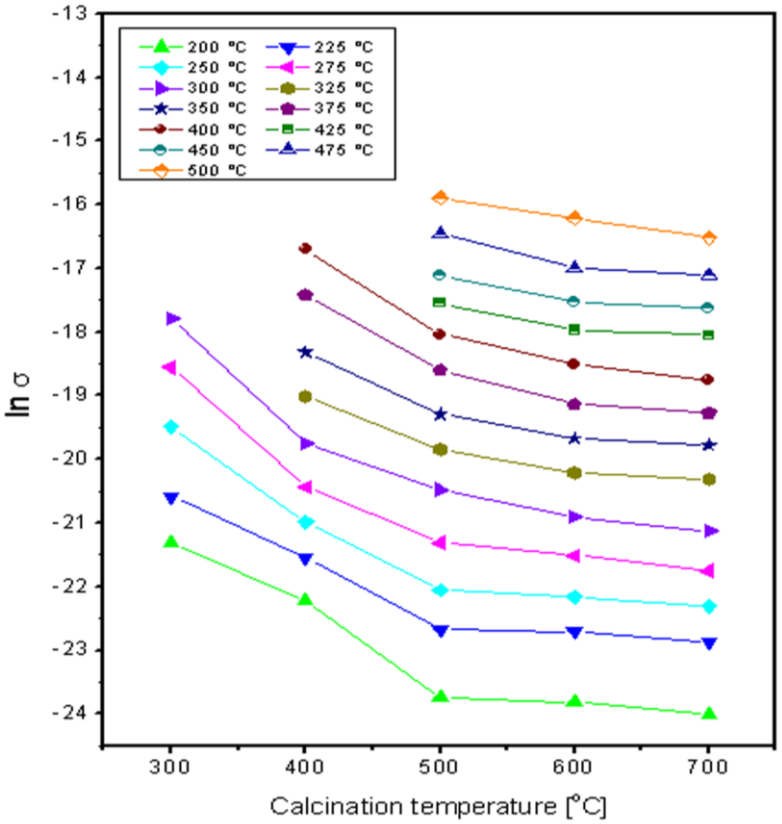

Figure 11. Variation of lnσ with the calcination temperature for erbia prepared using pH = 12.0 and calcined at the 300-700 °C.

This behavior can be understood taking into consideration: (i) the fact that increasing the pre-treatment temperature results in a continuous elimination of the traces of erbium carbonate as indicated by XPS analysis, and (ii) the increased crystallite size of Er_2O_3 during the calcination temperature raise. In agreement, a conductivity decrease was reported up on increasing the calcination temperature of Pr_6O_{11} from 600 to 700 °C [27] and for Dy_2O_3 from 500 to 700 °C [28]. This conductivity lowering was correlated with the obtained grain size decrease. Concurrently, higher conductivities at lower sintering temperatures were reported for Y_2O_3-doped CeO_2 ceramic [49].

4. CONCLUSIONS

In this contribution, we reported a simple and straightforward method, which involves the precipitation of erbium ions using sodium hydroxide, for the shape- and size-controlled synthesis of Er_2O_3 nanoparticles in high yield. It was found that the precipitation pH value as well as the calcination temperature are the key factors that controls the morphology, crystallite size, the electrical conductivity of the obtained Er_2O_3. Increasing the pH value during the precipitation has led to rod-like → sphere-like morphology transformation together with an increase in the inter-planer distances. Increasing the calcination temperature is accompanied by a crystallites size increase and a decrease in both the inter-planer distance and the electrical conductivity of the obtained solids.

ACKNOWLEDGEMENTS
This work was funded by the Center of Excellence for Advanced Materials Research (CEAMR), King Abdulaziz University, Jeddah under grant no. (CEAMR-SG-6-437). The authors, therefore, acknowledge with thanks CEAMR technical and financial support.

References

1. Z. K. Heiba, M. Bakr Mohamed and H. Fuess, *Cryst. Res. Technol.*, 47 (2012) 535.
2. N. D. Sharma, J. Singh, S. Dogra, D. Varandani, H. K. Poswal, S. M. Sharma and A. K. Bandyopadhyay, *J. Raman Spectrosc.*, 42 (2011) 438.
3. J. Pisarska, L. Žur, W.A. Pisarski, Phys. Status Solidi A 209 (2012) 1134.
4. S. Sato, R. Takahashi, M. Kobune, H. Inoue, Y. Izawa, H. Ohno and K. Takahashi, *Appl. Catal. A*, 356 (2009) 64.
5. A. Igarashi, S. Sato, R. Takahashi, T. Sodesawa and M. Kobune, *Catal. Commun.*, 8 (2007) 807.
6. H. Gotoh, Y. Yamada and S. Sato, *Appl. Catal. A*, 377 (2010) 92.
7. Z. Yanyan, F. Zebo and L. Yongsheng, *J. Rare Earths*, 28 (2010) 752.
8. C. Adelhelm, T. Pickert, M. Balden, M. Rasinski, T. Plocinski, C. Ziebert, F. Koch and H. Maier, *Scripta Mater.*, 61 (2009) 789.
9. C.H. Kao, H.C. Fan, S.N. Cheng and C.J. Liao, *Thin Solid Films*, 520 (2012) 3852.
10. M. M. Giangregorio, M. Losurdo, P. Capezzuto and G. Bruno, Appl. Surf. Sci., 255 (2009) 5396.
11. K. M. Hubbard and B.F. Espinoza, *Thin Solid Films*, 366 (2000) 175.
12. T. Tanaka, M. Yoshino, Y. Hishinuma D. Zhang, W. Kada, F. Sato, T. Iida, T. Nagasaki, T. Muroga, *J. Nucl. Mater.*, 417 (2011) 794.
13. T. Tanaka, B. Tsuchiya, F. Sato, T. Shikama, T. Iida and T. Muroga, *Fusion Eng. Des.*, 83 (2008) 1300.
14. T.-M. Pan, J.-C. Lin, M.-H. Wu and C.-S. Lai, *Sens. Actuators B*, 138 (2009) 619.
15. Z. B. Fang, Y. Y. Zhu, J. L. Wang and Z. M. Jiang, *Chin. Phys. B*, 18 (2009) 3542.
16. M. Losurdo, M. M. Giangregorio, M. Luchena, P. Capezzuto, G. Bruno, R. G. Toro, G. Malandrino, I. L. Fragala` and R. Lo Nigro, *Appl. Surf. Sci.*, 253 (2006) 322.
17. W. Zhong, H. X. Dai, C. F. Ng and C. T. Au, *Stud. Surf. Sci. Catal.*, 130 (2000) 1751.
18. T. Chikada, A. Suzuki, F. Koch, H. Maier, T. Terai and T. Muroga, *J. Nucl. Mater.*, 442 (2013) S592.
19. J. Yang, H. Chen, J. Zhang, S. Feng, M. Liu, G. Li, J. Ping, Q. Liu and Y. Yan, *Surf. Coat. Technol.*, 205 (2011) 5497.
20. Z. Li, H. Hahn and R.W. Siegel, *Mater. Lett.*, 6 (1988) 342.
21. H.R. Hoekstra and K.A. Gingerich, *Science*, 146 (1964) 1163.
22. R. Moon, W. Koehler, H. Child and R. Raubenheimer, *Phys. Rev.*, 176 (1968) 722.
23. J. Blanusa, B. Antic, A. Kremenovic, A.S. Nikolic, L. Mazzerolles, S. Mentus and V. Spasojevic, *Solid State Commun.*, 144 (2007) 310.
24. M. Lequitte and D. Autissier, *Nanostruct. Mater.*, 6 (1995) 333.
25. S. Hosokawa, S. Iwamoto and M. Inoue, *J. Alloys Compd.*, 457 (2008) 510.
26. Y. Wu, S. Zhu, T. Liu, F. Li, Y. Zhang, Y. Rao and Y. Zhang, *Appl. Surf. Sci.*, 307 (2014) 615.
27. B. M. Abu-Zied, Y. A. Mohamed and A. M. Asiri, *J. Rare Earths*, 31 (2013) 702.
28. B, M. Abu-Zied and A, M. Asiri, *J. Rare Earths*, 32 (2014) 259.
29. B. M. Abu-Zied, A. N. Mohamed and A. M. Asiri, *J. Nanosci. Nanotechnol.*, 15 (2015) 4487.
30. L. Song and M. Rongjun, *Asian J. Chem.*, 19 (2007) 1883.
31. N. Yanagihara, K. Vemulapalli, Q. Fernando and J.T. Dyke, *J. Less-Common Metals*, 167 (1991) 223.
32. M.S. Refat, *Synth. React. Inorg. Met.-Org. Chem.*, 34 (2004) 1605.

33. B. M. Abu-Zied, A. A. A. Farrag and A. M. Asiri, *Powder Technol.*, 246 (2013) 643.
34. K. Nagashima, H. Wakita and A. Mochizuki, *Bull. Chem. Soc. Jpn.*, 46 (1973) 152.
35. P. E. Caro, J. O. Sawyer and L. Eyring, *Spectrochim. Acta*, 28A (1972) 1167.
36. K. Michiba, T. Tahara, I. Nakai, R. Miyawaki and S. Matsubara, *Z. Kristallogr.*, 226 (2011) 518.
37. H. J. Won, S. H. Park, K. H. Kim and J. S. Choi, *J. Phys. Chem. Solids*, 48 (1987) 383.
38. K. M. Choi, K. H. Kim and J. S. Choi, *J. Phys. Chem. Solids*, 49 (1988) 1027.
39. Q. Li, J. Wang, Q.-Y. Xiang, T. Tang, Y.-C. Rao and J.-L. Cao, *Int. J. Hydrogen Energy*, 41 (2016) 3299.
40. R. Y. C. Tsai, L. Qian, H. Alizadeh and N. P. Kherani, *Optics Express*, 17 (2009) 21098.
41. T.-D. Nguyen, C.-T. Dinh and T.-O. Do, *ASC NANO*, 4 (2010) 2263.
42. R.-M. Lin, F.-C. Chu, A. Das, S.-Y. Liao, S.-T. Chou and L.-B. Chang, *Thin Solid Films*, 544 (2013) 526.
43. S. Zhu, Y. Wu, T. Liu, X. Wang, J. Yan and A. Yin, *Int. J. Hydrogen Energy*, 40 (2015) 5701.
44. H. H. Shen, S. M. Peng, X. G. Long, X. S. Zhou, L. Yang and X. T. Zu, *Vacuum*, 86 (2012) 1097.
45. B. M. Abu-Zied, S. M. Bawaked, S. A. Kosa and W. Schwieger, *Int. J. Electrochem. Sci.*, 11 (2016) 1568.
46. B. M. Abu-Zied, S. M. Bawaked, S. A. Kosa and W. Schwieger, *Int. J. Electrochem. Sci.*, 11 (2016) 2230.
47. K. H. Kim, D. Y. Yim, S. H. Park and J.S. Choi, *J. Phys. Chem. Solids*, 49 (1988) 151.
48. C. H. Yo, S. H. Park, J. S. Choi and M. S. Pyon, *J. Phys. Chem. Sotids*, 48 (1987) 733.
49. C. Tian and S. W. Chan, *Solid State Ionics*, 134 (2000) 89.